

ALMA Polarimetry of AT2018cow

KUIYUN HUANG,¹ JIRO SHIMODA,^{2,3} YUJI URATA,⁴ KENJI TOMA,^{2,3} KAZUTAKA YAMAOKA,^{5,6} KEIICHI ASADA,⁷
HIROSHI NAGAI,^{8,9} SATOKO TAKAHASHI,^{10,11,9} GLEN PETITPAS,¹² AND MAKOTO TASHIRO¹³

¹*Center for General Education, Chung Yuan Christian University, Taoyuan 32023, Taiwan*

²*Frontier Research Institute for Interdisciplinary Sciences, Tohoku University, Sendai 980-8578, Japan*

³*Astronomical Institute, Tohoku University, Sendai, 980- 8578, Japan*

⁴*Institute of Astronomy, National Central University, Chung-Li 32054, Taiwan*

⁵*Institute for Space-Earth Environmental Research (ISEE), Nagoya University, Furo-cho, Chikusa-ku, Nagoya, Aichi 464- 8601, Japan*

⁶*Division of Particle and Astrophysical Science, Graduate School of Science, Nagoya University, Furo-cho, Chikusa-ku, Nagoya, Aichi 464-8601, Japan*

⁷*Academia Sinica Institute of Astronomy and Astrophysics, Taipei 106, Taiwan*

⁸*National Astronomical Observatory of Japan, 2-21-1 Osawa, Mitaka Tokyo 181-8588, Japan*

⁹*Department of Astronomical Science, School of Physical Sciences, SOKENDAI (The Graduate University for Advanced Studies), Mitaka, Tokyo 181-8588, Japan*

¹⁰*Joint ALMA Observatory, Alonso de Córdova 3107, Vitacura, Santiago, Chile*

¹¹*NAOJ Chile Observatory, Alonso de Córdova 3788, Oficina 61B, Vitacura, Santiago, Chile*

¹²*Harvard-Smithsonian Center for Astrophysics, 60 Garden Street, Cambridge, Massachusetts 02138, USA*

¹³*Department of Physics, Saitama University, Shimo-Okubo, Saitama, 338-8570, Japan*

ABSTRACT

We present the first radio polarimetric observations of a fast-rising blue optical transient, AT2018cow. Two epochs of polarimetry with additional coincident photometry were performed with the Atacama Large Millimeter/submillimeter Array (ALMA). The overall photometric results based on simultaneous observations in the 100 and 230 GHz bands are consistent with the non-thermal radiation model reported by Ho et al. (2019) and indicate that the spectral peaks (~ 110 GHz at the first epoch and ~ 67 GHz at the second epoch) represent the synchrotron self-absorption frequency. The non-detection of linear polarization with $<0.15\%$ in the 230 GHz band at the phase when the effect of synchrotron self-absorption was quite small in the band may be explained by internal Faraday depolarization with high circumburst density and strong magnetic field. This result supports the stellar explosion scenario rather than the tidal disruption model. The maximum energy of accelerating particles at the shocks of AT2018cow-like objects is also discussed.

Keywords: transients — relativistic processes

1. INTRODUCTION

A luminous transient, AT2018cow, was discovered near the galaxy CGCG 137-068 ($z=0.0141$) at 2018-06-16 10:35:02 UT (Smartt et al. 2018). High luminosity in various wavelengths, featureless hot black-body spectra, and long-lived radio emission revealed that AT2018cow is an unusual transient (Rivera Sandoval et al. 2018; Prentice et al. 2018; Kuin et al. 2019; Ho et al. 2019). Panchromatic approaches suggested the presence of the central engine of high-energy emission radiated

through equatorial-polar asymmetric low-mass ejecta in a dense medium, and the progenitor of a low-mass H-rich star or blue supergiant star (Margutti et al. 2019; Soker et al. 2019; Ho et al. 2019). A scenario was also proposed in which a star disrupted by an intermediate black hole produced AT2018cow (Perley et al. 2019; Kuin et al. 2019). However, the large environment density concluded by Margutti et al. (2019); Ho et al. (2019) made the tidal disruption scenario unlikely and indicated a stellar explosion hypothesis. The host galaxy observation with HI 21cm mapping demonstrated that AT2018cow lies within an asymmetric ring of high column density, which indicates the formation of massive stars, supporting the stellar ex-

plosion scenario of AT2018cow (Roychowdhury et al. 2019). Lyutikov & Toonen (2018) built an electron-capture collapse model following a merger of white dwarfs one of which is a massive ONeMg white dwarf.

Polarimetry may be another key to investigating the circumstances of stellar explosion objects, such as density, magnetic field, and turbulence. Moreover, the study of particle acceleration at shocks associated with the objects could be equally interesting. For SN 1987A (Zanardo et al. 2018) and Kepler’s supernova remnant (SNR, DeLaney et al. 2002) as examples, spatially-resolved linear polarizations of radio synchrotron emissions were observed with local polarization degrees of $\sim 10\%$. The local polarization angles of both objects imply a radially oriented magnetic field. The polarization degree for integrated Stokes parameters over all emission regions is a few per cent. Such radial orientations and sizable polarization degrees are ubiquitously observed in young SNRs (such as the freely expanding phase to early Sedov phase, e.g. Milne 1987; Dickel et al. 1991 for Tycho’s SNR; Reynoso et al. 2013 for SN 1006) and could be explained by magnetohydrodynamic turbulence resulting from the interaction between the shock wave and density fluctuations pre-existing in the upstream medium (i.e. stellar wind and/or interstellar medium, Inoue et al. 2013). As for the early stages of radio supernovae, however, the density and magnetic field strength in the shocked region can be so high that the Faraday rotation effect is strong. Then the emissions from different parts in the shocked region have different polarization angles, which lead to suppression of the net linear polarization, i.e., the internal Faraday depolarization. The non-detection of linear polarization at 1.7–8.4 GHz in SN 1993J is explained by this effect (Bietenholz et al. 2003).

In this paper, we report the radio polarimetry of AT2018cow using the Atacama Large Millimeter/submillimeter Array (ALMA) in the 100 GHz and 230 GHz bands. In this millimeter wavelength range, the Faraday effect is weaker than the centimeter radio band. Based on two epochs of ALMA observations, the scenarios of a progenitor accompanied by a dense circumstellar medium are examined. MJD 58285 (2018-06-16 00:00:00 UT) is used as T_0 , which is between the last non-detection (MJD 58284.13) and the date of discovery (MJD 58285.441). The date is the same T_0 used in (Perley et al. 2019; Ho et al. 2019).

2. OBSERVATIONS

Two epochs of ALMA observations were executed as part of Director’s Discretionary Time (DDT) during Cycle 5 (2017.A.00046.T; PI K. Huang) using both

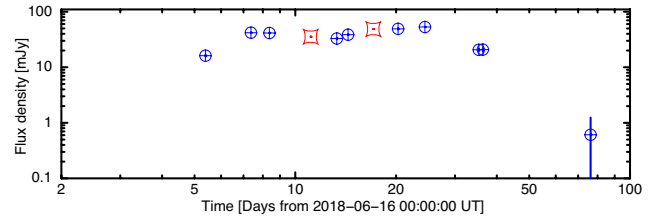


Figure 1. AT2018cow light curve in the submillimeter band (~ 230 GHz). The red box points indicate the photometric results of the ALMA and the blue circle points show the monitoring results reported by Ho et al. (2019).

the 12-m antenna array and Atacama Compact Array (ACA). The first epoch of radio linear polarimetry was performed at 97.5 GHz (i.e. Band3) starting at 27 June 2018 01:04 UT (midpoint $T_0=11.1$ d, here after epoch1). Coincident 230-GHz band (i.e. Band6) observations were also performed with the ACA. Because our quick-look photometry using the ACA data exhibited the brightness sufficient for polarimetry and positive power-law index by fitting with $f_\nu \propto \nu^\beta$, we decided to switch the frequency from Band3 to Band6 to perform polarimetry above the spectral peak. Hence, the second epoch of polarimetry was executed at the 230 GHz band using the 12-m antenna array on 3 July 2018 UT (midpoint $T_0=17.1$ d, here after epoch2). The coincident photometry at 97.5 GHz was also performed using the ACA. For the 12-m antenna array, the bandpass and flux were calibrated using observations of J1550+0527, and J1606+1814 was used for the phase calibration. Polarization calibration was performed by observations of J1642+3948. Regarding ACA observations, J1337-1257 and J1517-2422 were utilized for the bandpass and flux calibrations. The phase calibrations were performed using observations of J1540+1447, J1613+3412, and J1619+2247.

3. ANALYSIS AND RESULTS

The raw data of ALMA were reduced at the East Asian ALMA Regional Center (EA-ARC) using CASA (version 5.1.1) (McMullin et al. 2007). We further performed interactive CLEAN deconvolution imaging (Högbom 1974; Clark 1980) with self-calibration for the data obtained by the 12-m antenna array. The Stokes I , Q , and U maps were CLEANed with an appropriate number of CLEAN iterations after the final round of self-calibration. The results of photometry and polarimetry are summarized in Table 1. Regarding polarimetry, the $3\text{-}\sigma$ upper limits were derived based on the non-detections in Q and U maps. Because the depolarization between the source and observation site is negligible for the point source (i.e., transients) in this millimeter band (Brentjens & Faraday 2005), the val-

ues of $< 0.10\%$ in the 97.5-GHz band and $< 0.15\%$ in the 233-GHz band describe the intrinsic origin.

To describe the phase of the polarization observation, the photometric measurements in the entire Band6 frequency range were plotted, together with the 230-GHz monitoring data (Ho et al. 2019). As shown in Figure 1, the ~ 230 -GHz light curves indicate that our polarimetric measurements were performed around the brightest plateau phase with significant variabilities.

The photometric measurements in each of the spectral windows (SPWs) of Band3 and Band6 were fitted with a simple power-law function (i.e. $f_\nu \propto \nu^\beta$). These fittings yield $\beta_{E1B3} = 1.080 \pm 0.007$ ($\chi^2/ndf=1.39$ with number of degree of freedom, $ndf=2$) for epoch1 with Band3, $\beta_{E1B6} = -1.15 \pm 0.16$ ($\chi^2/ndf=0.62$ with $ndf=2$) for epoch1 with Band6, $\beta_{E2B3} = 0.44 \pm 0.05$ ($\chi^2/ndf=1.00$ with $ndf=2$) for epoch2 with Band3, and $\beta_{E2B6} = -0.86 \pm 0.29$ ($\chi^2/ndf=280$ with $ndf=2$) for epoch2 with Band6. Large scatter were observed at 242 GHz (i.e. the highest frequency in Band6) for epoch2, which may be related to the significant variabilities as shown in Figure 1. The same fitting was therefore performed by excluding the data, and $\beta_{E2B6} = -0.65 \pm 0.02$ ($\chi^2/ndf=1.25$ with $ndf=1$) was obtained. As shown in Figure 2, the fitting basically describes the spectral energy distribution (SED) and indicates that the spectral peak frequency, ν_p is located at ~ 140 GHz. Hence, the polarimetric measurements on epoch1 and epoch2 were performed below and above the spectral peak, respectively.

4. DISCUSSION

4.1. Spectral Flux Distribution

The observed radio light curves and time-resolved spectra of AT2018cow may be interpreted as the synchrotron emission of relativistic non-thermal electrons produced at an adiabatic strong shock that freely expands in an ionized medium at a non-relativistic speed (Ho et al. 2019; Margutti et al. 2019). This emission model is widely applicable for radio supernovae (Chevalier 1998). Considering the smooth connection of two power-law spectra, the temporal evolution of the spectral indices in Band 3 may be consistent with the spectral modeling presented by Ho et al. (2019). The smooth broken power-law fitting was performed, including ATCA data taken at the similar epochs ($\Delta t = -0.6$ d for epoch1 and $\Delta t = 0.4$ d for epoch2 (Ho et al. 2019)). The smooth fitting with wider spectral frequency coverage is also reasonable to characterize the spectral peak frequency as the method is applied for various analyses such as GRB prompt emissions (e.g. Band et al. 1993). Because the significant variabilities were observed (Fig-

ure 1), we excluded the data taken by the Submillimeter Array (SMA). For this fitting, the spectral index of the lower-frequency side was fixed as $\beta_{low} = 2.5$ (reported by Ho et al. (2019)), and the higher-frequency side was fixed as $\beta_{high} = -1.15$ for epoch1 and $\beta_{high} = -0.86$ for epoch2. The fitting yields the spectral peak frequency, $\nu_p = 109.8 \pm 0.5$ GHz ($\chi^2/ndf=7.3$ with $ndf=7$) at epoch1 and $\nu_p = 67.4 \pm 1.6$ GHz ($\chi^2/ndf=7.6$ with $ndf=6$) at epoch2¹. The larger reduced χ^2 may be caused by the epoch differences. As show in Figure 3, the best-fit functions basically describe the SED. The temporal evolution of the spectral peak frequency is also characterized as $\nu_p \propto t^{-1.1}$, which is consistent with that of the theoretical model for the synchrotron self-absorption frequency (Chevalier 1998). Therefore, we concluded that the spectral peak frequency represents the synchrotron self-absorption frequency, and the effect of self-absorption is quite small for the polarization measurement with in the 233-GHz band at epoch2.

For further discussion in §4.2, the theoretical analysis of Ho et al. (2019) is followed for the estimated values of the radius of the shock, magnetic field strength in the shocked region, shock speed, and number density of the shocked region at $T \simeq 22$ d as

$$R \simeq 7 \times 10^{15} \left(\frac{\epsilon_e f}{\epsilon_B 0.5} \right)^{-\frac{1}{19}} \left(\frac{F_p}{94 \text{ mJy}} \right)^{\frac{9}{19}} \times \left(\frac{D}{60 \text{ Mpc}} \right)^{\frac{18}{19}} \left(\frac{\nu_p}{100 \text{ GHz}} \right)^{-1} \text{ cm}, \quad (1)$$

$$B \simeq 6 \left(\frac{\epsilon_e f}{\epsilon_B 0.5} \right)^{-\frac{4}{19}} \left(\frac{F_p}{94 \text{ mJy}} \right)^{-\frac{2}{19}} \times \left(\frac{D}{60 \text{ Mpc}} \right)^{-\frac{4}{19}} \left(\frac{\nu_p}{100 \text{ GHz}} \right) \text{ G}, \quad (2)$$

$$\frac{v}{c} \simeq 0.1 \left(\frac{\epsilon_e f}{\epsilon_B 0.5} \right)^{-\frac{1}{19}} \left(\frac{F_p}{94 \text{ mJy}} \right)^{\frac{9}{19}} \times \left(\frac{D}{60 \text{ Mpc}} \right)^{\frac{18}{19}} \left(\frac{\nu_p}{100 \text{ GHz}} \right)^{-1} \left(\frac{T}{22 \text{ day}} \right)^{-1} \quad (3)$$

$$n_e \simeq 1 \times 10^5 \frac{1}{\epsilon_B} \left(\frac{\epsilon_e f}{\epsilon_B 0.5} \right)^{-\frac{6}{19}} \left(\frac{F_p}{94 \text{ mJy}} \right)^{-\frac{22}{19}} \times \left(\frac{D}{60 \text{ Mpc}} \right)^{-\frac{44}{19}} \left(\frac{\nu_p}{100 \text{ GHz}} \right)^4 \left(\frac{T}{22 \text{ day}} \right)^2 \text{ cm}^{-3} \quad (4)$$

¹ The differences between our deduced spectral peak frequencies and ~ 100 GHz at 22 day estimated by Ho et al. (2019) may be caused by their analysis for narrow frequency range and power-law index measurement (-1.06 ± 0.01) using interpolated SMA data (between 20 d and 24 d). Much flatter spectral index may be reasonable to explain the spectral excess of their measurement with 671 GHz at 23 d.

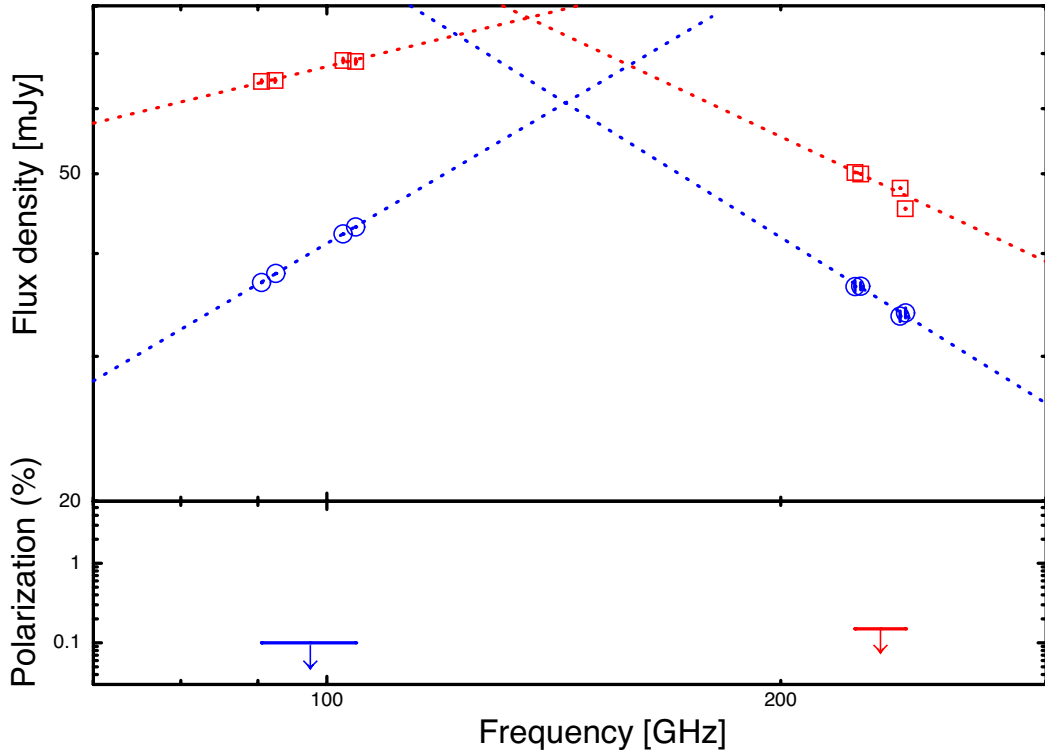


Figure 2. SED and polarization using ALMA Band3 and Band6 data taken at 11.1 (blue circle points and arrow) and 17.1 (red box points and arrow) d. The blue and red dotted lines indicate the best fitted simple power-law functions.

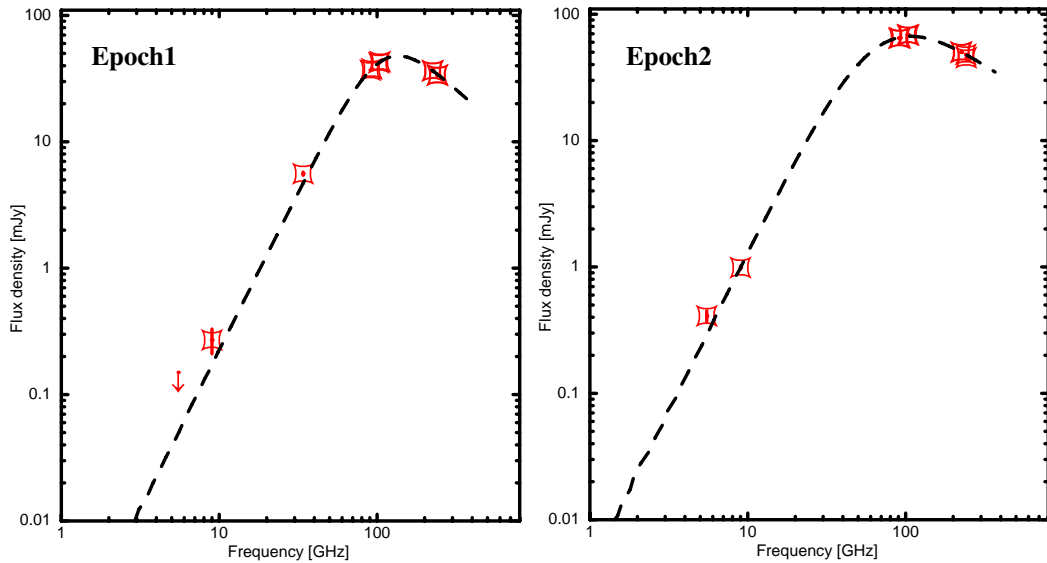


Figure 3. SED of the AT2018cow at 11.1 d (i.e., epoch1, left) and 17.1 d (i.e., epoch2, right) using ALMA with the ATCA data taken by Ho et al. (2019). Time differences of ATCA observations were $\Delta t = -0.6$ d for epoch1 and $\Delta t = 0.4$ d for epoch2, respectively. The dashed lines indicate the best fit smoothly connected broken power-law functions with the spectral peak frequencies of ~ 110 GHz at epoch1 and ~ 67 GHz at epoch2.

where ϵ_e and ϵ_B are the fractions of thermal energy at the shocked region that are carried by the non-thermal electrons and the magnetic field, respectively, and f is the filling factor of the emission region in the sphere with radius R .

4.2. Polarization

As introduced in §1, the polarization degree of AT2018cow without the Faraday effect is expected to be a few percent, which is similar to other stellar explosions². The non-detection of linear polarization (especially $<0.15\%$ in the 233-GHz band at epoch2) in AT2018cow may be explained by internal Faraday depolarization, because n_e and B are so high. The result supports the stellar explosion scenario rather than the tidal disruption scenario³.

In this scenario, we can derive a lower limit of the coherence length of the turbulent magnetic field in the shocked region. Supposing that the turbulent magnetic energy peaks at the maximum coherence length scale ℓ_M , which is observationally implied in Tycho's SNR (Shimoda et al. 2018), we obtain the Faraday depth as

$$\tau_V = \frac{e^3}{\pi m_e^2 c^2} n_e \frac{B}{\sqrt{N}} R \nu^{-2}, \quad (5)$$

where $N \sim R/\ell_M$. The condition $\tau_V > 1$ at $\nu \sim 100$ GHz gives

$$\begin{aligned} \ell_M > \ell_V &\equiv \left(\frac{\pi m_e^2 c^2}{e^3} \frac{\nu^2}{n_e B \sqrt{R}} \right)^2 \\ &= 2 \times 10^6 \left(\frac{n_e}{3 \times 10^5 \text{ cm}^{-3}} \right)^{-2} \left(\frac{B}{6 \text{ G}} \right)^{-2} \\ &\quad \times \left(\frac{R}{7 \times 10^{15} \text{ cm}} \right)^{-1} \left(\frac{\nu}{100 \text{ GHz}} \right)^4 \text{ cm} \end{aligned} \quad (6)$$

The observation of Tycho's SNR indicates $\ell_M \sim R/10$ (Shimoda et al. 2018). If this relation is valid for AT2018cow, the values of n_e , B , and R estimated by Ho et al. (2019) and Margutti et al. (2019) (Eqs. 1, 2, and 4) satisfy Eq. (6).

The lower limit on ℓ_M leads to the lower limit on the maximum energy of accelerating particles at the shock.

² The optical linear polarizations were detected (Smith et al. 2018) when the thermal radiation dominated in the optical range (Perley et al. 2019; Margutti et al. 2019). Hence, the values are not appropriate to refer to as the polarization degree without the Faraday depolarization effect.

³ In the tidal disruption scenario, the external shock which propagates in the interstellar medium will have $n_e \sim 1 \text{ cm}^{-3}$, $B \sim 1 \mu\text{G}$ (Perley et al. 2019; Gaensler et al. 2005), $R < c \times 22$ day. These lead to $\tau_V < 3 \times 10^{-7} \ll 1$ in Eq. (5) even for $N = 1$, and then a sizable linear polarization may be detected.

In the first-order Fermi acceleration, which is assumed by Ho et al. (2019), energetic particles are scattered through interactions with the turbulent magnetic-field to go back and forth between upstream and downstream of the shock, and then gain energies at every reciproca-tion (Bell 1978; Blandford & Ostriker 1978). The particles experience large angle scattering if they resonantly interact with magnetic disturbances with a scale length comparable to their gyro radius, i.e. a pitch-angle scattering (Jokipii 1966). When the gyro radius of accelerated particles becomes larger than the maximum coherence length scale ℓ_M , the particle is no longer efficiently scattering and escapes from the shock. Thus, we obtain the maximum energy of accelerating particles as

$$\begin{aligned} E_{\max} &> e B \ell_V \\ &\simeq 3 \left(\frac{n_e}{3 \times 10^5 \text{ cm}^{-2}} \right)^{-2} \left(\frac{B}{6 \text{ G}} \right)^{-1} \\ &\quad \times \left(\frac{R}{7 \times 10^{15} \text{ cm}} \right)^{-1} \left(\frac{\nu}{100 \text{ GHz}} \right)^4 \text{ GeV}. \end{aligned} \quad (7)$$

This argument is consistent with the model in which the relativistic non-thermal electrons are produced by the shock in AT2018cow.

The strong ν dependence of the lower limit on E_{\max} should be emphasized. If one can perform polarimetric observation of such kinds of stellar explosions at higher frequencies, a stricter limit on E_{\max} can be obtained. The origin of the PeV energy cosmic-rays is unknown. By polarimetry at a higher ν (i.e. $\sim\text{THz}$), we could examine whether AT2018cow-like objects are the origin of PeV cosmic-rays.

This paper makes use of the following ALMA data: ADS/JAO.ALMA#2017.A.00046.T. ALMA is a partnership of ESO (representing its member states), NSF (USA) and NINS (Japan), together with NRC (Canada), MOST and ASIAA (Taiwan), and KASI (Republic of Korea), in cooperation with the Republic of Chile. The Joint ALMA Observatory is operated by ESO, AUI/NRAO and NAOJ. This work is supported by the Ministry of Science and Technology of Taiwan grants MOST 105-2112-M-008-013-MY3 (Y.U.) and 106-2119-M-001-027 (K.A.). This work is also supported by JSPS Grants-in-Aid for Scientific Research No. 18H01245 (K.T.). We thank EA-ARC, especially Pei-Ying Hsieh for support in the ALMA observations. Y.U., K. Y. H., and K. A. also thank Ministry of Education Republic of China.

Facilities: ALMA

Software: CASA (McMullin et al. 2007)

REFERENCES

- Band, D., Matteson, J., Ford, L., et al. 1993, *ApJ*, 413, 281
- Bell, A. R. 1978, *MNRAS*, 182, 147
- Bietenholz, M. F., Bartel, N., & Rupen, M. P. 2003, *ApJ*, 597, 374
- Blandford, R. D., & Ostriker, J. P. 1978, *ApJL*, 221, L29
- Brentjens, M.A. & de Bruyn, A. G. *Faraday Astron. Astrophys.* 441, 1217-1228 (2005)
- Chevalier, R. A. 1998, *ApJ*, 499, 810
- Clark, B. G. 1980, *A&A*, 89, 377
- DeLaney, T., Koralesky, B., Rudnick, L., & Dickel, J. R. 2002, *ApJ*, 580, 914
- Dickel, J. R., van Breugel, W. J. M., & Strom, R. G. 1991, *AJ*, 101, 2151
- Gaensler, B. M., Haverkorn, M., Staveley-Smith, L., et al. 2005, *Science*, 307, 1610
- Ho, A. Y. Q., Phinney, E. S., Ravi, V., et al. 2019, *ApJ*, 871, 73
- Högbom, J. A. 1974, *A&AS*, 15, 417
- Inoue, T., Shimoda, J., Ohira, Y., & Yamazaki, R. 2013, *ApJL*, 772, L20
- Jokipii, J. R. 1966, *ApJ*, 146, 480
- Kuin, N. P. M., Wu, K., Oates, S., et al. 2019, *MNRAS*, Lyutikov, M., & Toonen, S. 2018, arXiv:1812.07569
- Margutti, R., Metzger, B. D., Chornock, R., et al. 2019, *ApJ*, 872, 18
- McMullin, J. P., Waters, B., Schiebel, D., Young, W., & Golap, K. 2007, *Astronomical Data Analysis Software and Systems XVI*, 376, 127
- Milne, D. K. 1987, *Australian Journal of Physics*, 40, 771
- Perley, D. A., Mazzali, P. A., Yan, L., et al. 2019, *MNRAS*, 484, 1031
- Prentice, S. J., Maguire, K., Smartt, S. J., et al. 2018, *ApJL*, 865, L3
- Reynoso, E. M., Hughes, J. P., & Moffett, D. A. 2013, *AJ*, 145, 104
- Rivera Sandoval, L. E., Maccarone, T. J., Corsi, A., et al. 2018, *MNRAS*, 480, L146
- Roychowdhury, S., Arabsalmani, M., & Kanekar, N. 2019, *MNRAS*, 485, L93
- Shimoda, J., Akahori, T., Lazarian, A., Inoue, T., & Fujita, Y. 2018, *MNRAS*, 480, 2200
- Smartt, S. J., Clark, P., Smith, K. W., et al. 2018, *The Astronomer's Telegram*, 11727,
- Smith, P. S., Leonard, D. C., Bilinski, C., et al. 2018, *The Astronomer's Telegram*, 11789
- Soker, N., Grichener, A., & Gilkis, A. 2019, *MNRAS*, 484, 4972
- Zanardo, G., Staveley-Smith, L., Gaensler, B. M., et al. 2018, *ApJL*, 861, L9

Table 1. ALMA Observing Log

Epoch1: 2018-06-27 01:04-04:43, $T_0=11.1$ d (midpoint)							
Instruments	SPW	Band [GHz]	Pol. [%]	P.A [deg]	I flux [mJy]	Q flux [mJy]	U flux [mJy]
12m	0,1,2,3	97.5	< 0.10	–	39.629±0.046	0.010 (rms)	0.010 (rms)
	0	90.5	< 0.18	–	36.886±0.029	0.016 (rms)	0.014 (rms)
	1	92.5	< 0.17	–	37.823±0.029	0.016 (rms)	0.015 (rms)
	2	102.5	< 0.15	–	42.243±0.030	0.015 (rms)	0.015 (rms)
	3	104.5	< 0.17	–	43.087±0.036	0.017 (rms)	0.017 (rms)
Epoch1: 2018-06-27 01:00-04:05, $T_0=11.1$ d (midpoint)							
Instruments	SPW	Band [GHz]	Pol. [%]	P.A [deg]	I flux [mJy]	Q flux [mJy]	U flux [mJy]
ACA	4,6,16,18	233.0	–	–	35.49±0.48	–	–
	4	224.0	–	–	36.47±0.57	–	–
	6	226.0	–	–	36.51±0.37	–	–
	16	240.0	–	–	33.57±0.49	–	–
	18	242.0	–	–	33.88±0.47	–	–
Epoch2: 2018-07-03 00:39-02:06, $T_0=17.1$ d (midpoint)							
Instruments	SPW	Band [GHz]	Pol. [%]	P.A [deg]	I flux [mJy]	Q flux [mJy]	U flux [mJy]
ACA	4,6,8,10	97.5	–	–	68.18±0.44	–	–
	4	90.5	–	–	64.74±0.31	–	–
	6	92.4	–	–	64.93±0.37	–	–
	8	102.5	–	–	68.66±0.45	–	–
	10	104.5	–	–	68.47±0.53	–	–
Epoch2: 2018-07-03 00:43-04:05, $T_0=17.1$ d (midpoint)							
Instruments	SPW	Band [GHz]	Pol. [%]	P.A [deg]	I flux [mJy]	Q flux [mJy]	U flux [mJy]
12m	0,1,2,3	232.9	< 0.15	–	48.755±0.047	0.016 (rms)	0.018 (rms)
	0	224.0	< 0.23	–	50.186±0.052	0.025 (rms)	0.028 (rms)
	1	226.0	< 0.22	–	49.975±0.046	0.026 (rms)	0.025 (rms)
	2	240.0	< 0.25	–	48.023±0.050	0.027 (rms)	0.029 (rms)
	3	242.0	< 0.31	–	45.348±0.086	0.033 (rms)	0.033 (rms)